Insulin receptor substrate 2 plays a crucial role in β cells and the hypothalamus

Naoto Kubota,[1,2,3,4] Yasuo Terauchi,[1,2] Kazuyuki Tobe,[1,2] Wataru Yano,[1] Ryo Suzuki,[1,2] Kohjiro Ueki,[1] Iseki Takamoto,[1,2] Hidemi Satoh,[1] Toshiyuki Maki,[1] Tetsuya Kubota,[5] Masao Moroi,[5] Miki Okada-Iwabu,[4] Osamu Ezaki,[6] Ryozo Nagai,[7] Yoichi Ueta,[8] Takashi Kadowaki,[1,2,4] and Tetsuo Noda[3,9]

[1]Department of Metabolic Diseases, Graduate School of Medicine, University of Tokyo, Tokyo, Japan. [2]Core Research for Evolutional Science and Technology (CREST), Japan Science and Technology Corporation, Saitama, Japan. [3]Department of Cell Biology, Japanese Foundation for Cancer Research — Cancer Institute, Tokyo, Japan. [4]Division of Applied Nutrition, National Institute of Health and Nutrition, Tokyo, Japan. [5]Third Department of Internal Medicine, Toho University School of Medicine, Ohashi Hospital, Tokyo, Japan. [6]Division of Clinical Nutrition, National Institute of Health and Nutrition, Tokyo, Japan. [7]Department of Cardiovascular Diseases, Graduate School of Medicine, University of Tokyo, Tokyo, Japan. [8]Department of Physiology, School of Medicine, University of Occupational and Environmental Health, Kitakyushu, Japan. [9]Department of Molecular Genetics, Tohoku University School of Medicine, Sendai, Japan.

We previously demonstrated that insulin receptor substrate 2 (Irs2) KO mice develop diabetes associated with hepatic insulin resistance, lack of compensatory β cell hyperplasia, and leptin resistance. To more precisely determine the roles of Irs2 in β cells and the hypothalamus, we generated β cell–specific Irs2 KO and hypothalamus-specific Irs2 knockdown (βHT-IRS2) mice. Expression of Irs2 mRNA was reduced by approximately 90% in pancreatic islets and was markedly reduced in the arcuate nucleus of the hypothalamus. By contrast, Irs2 expression in liver, muscle, and adipose tissue of βHT-IRS2 mice was indistinguishable from that of control mice. The βHT-IRS2 mice displayed obesity and leptin resistance. At 4 weeks of age, the βHT-IRS2 mice showed normal insulin sensitivity, but at 8 and 12 weeks, they were insulin resistant with progressive obesity. Despite their normal insulin sensitivity at 8 weeks with caloric restriction, the βHT-IRS2 mice exhibited glucose intolerance and impaired glucose-induced insulin secretion. β Cell mass and β cell proliferation in the βHT-IRS2 mice were reduced significantly at 8 and 12 weeks but not at 10 days. Insulin secretion, normalized by cell number per islet, was significantly increased at high glucose concentrations in the βHT-IRS2 mice. We conclude that, in β cells and the hypothalamus, Irs2 is crucially involved in the regulation of β cell mass and leptin sensitivity.

Introduction

The pathogenesis of type 2 diabetes involves complex interactions among multiple physiological defects. Transgenic and KO technologies that allow the creation of animal models of type 2 diabetes have had a major impact on the assessment of newly identified molecules implicated in the regulation of glucose homeostasis in vivo (1). Insulin receptor substrates 1 and 2 (Irs1 and Irs2) are 2 major substrates for insulin receptor tyrosine kinase and IGF receptor kinase (2–6), and the physiological roles of these proteins have been evaluated by gene targeting strategies (7). Irs1 KO (*Irs1*−/−) mice are growth-retarded and insulin-resistant (8, 9) but because of compensatory hyperinsulinemia associated with β cell hyperplasia in response to insulin resistance, they do not develop diabetes (10).

Irs2−/− mice, on the other hand, develop type 2 diabetes associated with hepatic insulin resistance, lack of compensatory β cell hyperplasia, and leptin resistance (11–14). In fact, we previously reported that at 6 and 12 weeks of age, β cell mass in *Irs2*−/− mice was reduced to 83% and 51%, respectively, of that in WT mice (13). The *Irs2*−/− mice displayed leptin resistance; and a low dose of leptin

that was adequate to reduce food intake and body weight in WT mice had no effect in *Irs2*−/− mice (14). However, since insulin resistance caused by the absence of Irs2 in peripheral tissues may affect leptin sensitivity and β cell proliferation, disruption of the *Irs2* gene specifically in β cells and the hypothalamus would be required to more precisely determine the roles of Irs2 at these sites. In the present study, we generated β cell–specific Irs2 KO and hypothalamus-specific Irs2 knockdown (βHT-IRS2) mice by crossing Irs2 floxed mice (*Irs2lox/lox*) and transgenic mice expressing Cre under control of the rat insulin II promoter (RIP-Cre mice). Expression of Irs2 mRNA in the βHT-IRS2 mice was reduced by approximately 90% in the islets and markedly reduced in the arcuate nucleus of the hypothalamus, whereas liver, muscle and adipose tissue expressions in βHT-IRS2 and control mice were indistinguishable. The βHT-IRS2 mice were obese and leptin resistant. Furthermore, despite normal insulin sensitivity, these mice also displayed glucose intolerance and impaired glucose-induced insulin secretion. Both β cell mass and β cell proliferation in the βHT-IRS2 mice were significantly reduced at 8 and 12 weeks, but not at 10 days, and insulin secretion in these mice, normalized by cell number per islet, was significantly increased at high glucose concentrations. In conclusion, Irs2 in β cells and the hypothalamus plays crucial roles in the regulation of β cell mass and leptin sensitivity.

Results

Generation of βHT-IRS2 mice. Irs2lox/lox mice were generated by homologous recombination (Figure 1, A and B). We first performed a genomic DNA PCR analysis to detect Cre-mediated recombination at the genomic DNA level. Irs2 alleles were not deleted in any of

the tissues of the *Irs2*[lox/lox] mice (Figure 1C), but they were almost completely deleted in the islets and partially (50%) deleted in the hypothalami of *Irs2*[lox/lox]/RIP-Cre mice (Figure 1C). Next, we investigated the expression levels of Cre mRNA and Irs2 mRNA in the livers, skeletal muscles, adipose tissues, hypothalami, and pancreatic islets of WT, RIP-Cre, *Irs2*[lox/lox], and *Irs2*[lox/lox]/RIP-Cre mice. RT-PCR detected Cre mRNA expression in pancreatic β cells of the RIP-Cre and *Irs2*[lox/lox]/RIP-Cre mice, but not in hepatic, skeletal muscle, or adipose tissues (Figure 1D). Although Cre recombinase was under the control of the rat insulin II promoter, Cre mRNA was also detected in the hypothalami of the *Irs2*[lox/lox]/RIP-Cre and RIP-Cre mice (Figure 1D), suggesting that Irs2 deletion had also occurred in the hypothalamus. In fact, although no differences in Irs2 mRNA levels between genotypes were detected in hepatic, skeletal muscle or adipose tissues (Figure 1D), Irs2 mRNA levels in islets were markedly reduced in the *Irs2*[lox/lox]/RIP-Cre mice (Figure 1D), and Irs2 mRNA levels in the hypothalamus were partially (50%) reduced in the *Irs2*[lox/lox]/RIP-Cre mice (Figure 1D). These findings indicate that the *Irs2*[lox/lox]/RIP-Cre mice were βHT-IRS2 mice.

Given the similar expression levels of Irs2 in β cells and the hypothalamus among WT, RIP-Cre, and *Irs2*[lox/lox] mice, which indicates that neither insertion of the loxP and neomycin-resistance gene (*neoR*) sites nor expression of Cre recombinase alone affected the abundance of Irs2, we performed subsequent experiments using *Irs2*[lox/lox] (control) and βHT-IRS2 mice. Irs2 protein was not detected in islets and was partially (50%) reduced in the hypothalami of βHT-IRS2 mice (Figure 1E).

βHT-IRS2 mice show leptin resistance. The body weight of the βHT-IRS2 mice was significantly higher than that of the control mice from 5 weeks onward (Figure 2A). The white adipose tissue (WAT) mass of the epididymal fat pads was also significantly higher in

Figure 1

Generation of βHT-IRS2 mice. (**A**) Schematic representation of the 3 steps in our gene-targeting strategy. (**B**) Southern blot analysis. Left: *Sac*I-digested ES cell genomic DNA hybridized with probe A. The 4-kb band corresponds to the WT (+) allele, and the 3.2-kb band to the first step of the mutant (neo) allele. Middle: *Spe*I- and *Eco*RV-digested ES cell genomic DNA hybridized with probe B. The 11.8-kb band corresponds to the WT (+) allele, the 2.9-kb band to the (neo) allele, and the 1.6-kb band to the second step of the mutant (Δ) allele. Right: *Hind*III-digested ES cell genomic DNA hybridized with probe C. The 17.3-kb band corresponds to the WT (+) allele, the 15.2-kb band to the mutant (Δ) allele, and the 6-kb band to final step of the mutant (neoΔ) allele. (**C**) PCR analysis of genomic DNA to detect Cre-mediated recombination. K, kidney; L, liver; M, muscle; A, adipose tissue; S, spleen; HT, hypothalamus; H, heart; Lu, lung; I, islet. (**D**) RT-PCR of Cre and Irs2 expression in liver, skeletal muscle, adipose tissue, hypothalami, and pancreatic islets of WT, RIP-Cre, *IRS2*[lox/lox], and *IRS2*[lox/lox]/RIP-Cre (βHT-IRS2) mice. (**E**) Western blot analysis of Irs2 in pancreatic islets (upper panel) and hypothalami (lower panel) from control and βHT-IRS2 mice.
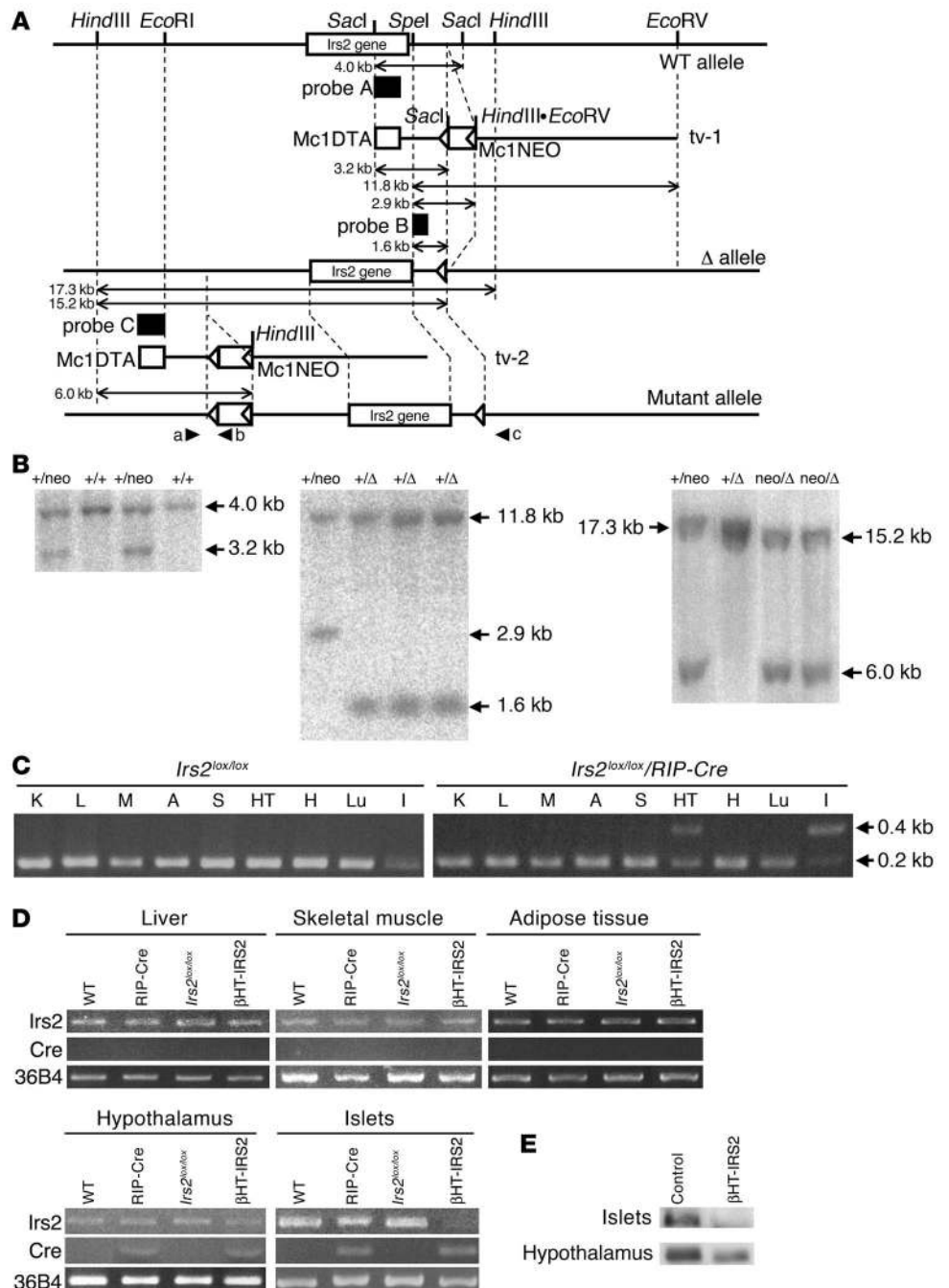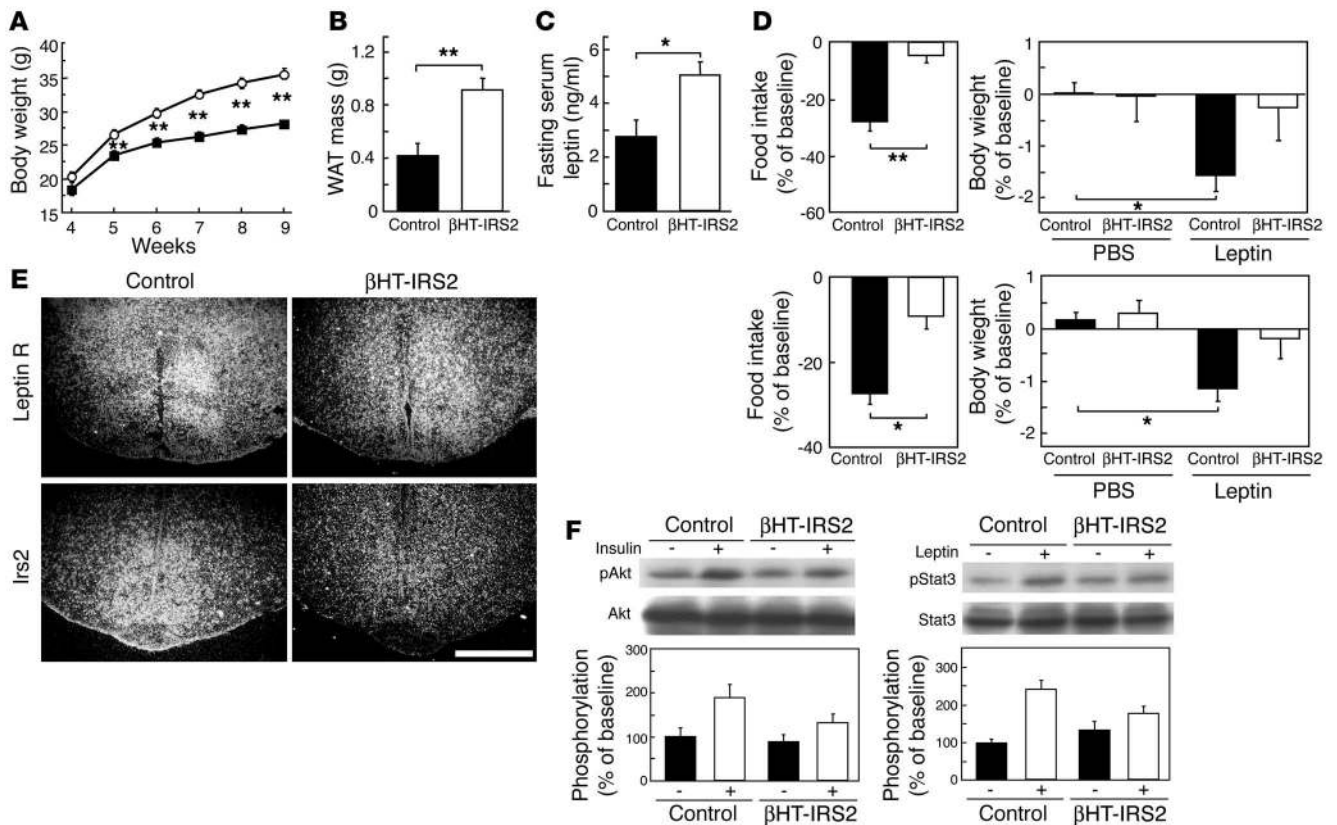
Figure 2
βHT-IRS2 mice showed leptin resistance. (**A**) Body weights of control and βHT-IRS2 mice. Values are means ± SE of data obtained from the analysis of control (filled squares, *n* = 10) and βHT-IRS2 mice (open circles, *n* = 11). (**B**) WAT mass of epididymal fat pads of control and βHT-IRS2 mice at 12 weeks. Values are means ± SE of data obtained from the analysis of control (black bar, *n* = 5) and βHT-IRS2 mice (white bar, *n* = 9). (**C**) Fasting serum leptin levels of control and βHT-IRS2 mice at 8 weeks. Values are means ± SE of data obtained from the analysis of control (black bar, *n* = 10) and βHT-IRS2 mice (white bar, *n* = 11). (**D**) Leptin-mediated suppression of food intake (left) and body weight (right) at 8 weeks. Baseline food intake was measured during PBS injection. Values are means ± SE of data obtained from the analysis of control (black bar, *n* = 9) and βHT-IRS2 mice (white bar, *n* = 7). (**E**) In situ hybridization of the leptin receptor and Irs2 in hypothalami from control and βHT-IRS2 mice. Scale bar represents 1 mm. (**F**) Insulin-stimulated phosphorylation of Akt (top) and leptin-stimulated phosphorylation of Stat3 (bottom). Upper panels: lysates from untreated and insulin-treated mice were immunoblotted for anti–phospho-Akt (pAkt) and anti-Akt. Lower panels: lysates from untreated and leptin-treated mice were immunoblotted for anti–phospho-Stat3 (pStat3) and anti-Stat3. In graphs, white bars represent insulin- (left) or leptin- (right) stimulated phosphorylation. Data (means ± SE) are representative of at least 3 independent experiments. *P < 0.05; **P < 0.01.

the βHT-IRS2 mice than in the control mice at 12 weeks (Figure 2B). At 8 weeks, fasting serum leptin levels were significantly higher in βHT-IRS2 mice than in control mice (Figure 2C), suggesting the former to be leptin-resistant. To assess leptin sensitivity directly, we compared the responses of βHT-IRS2 mice and control mice to exogenous leptin. Suppression of food intake was significantly smaller in the βHT-IRS2 mice than in the control mice, and body weight was significantly suppressed in the control mice, but not in the βHT-IRS2 mice (Figure 2D, upper panels). To rule out the possibility that this leptin resistance may be secondary to obesity, we next assessed leptin sensitivity in 8-week-old βHT-IRS2 mice that were pair-fed with control mice for 4 weeks, starting from 4 weeks of age. Pair-fed βHT-IRS2 mice did not become obese; their body weights were identical to those of controls. Suppression of food intake was significantly reduced in the βHT-IRS2 mice as compared with the control mice, and body weight was significantly suppressed in the control mice, but not in the βHT-IRS2 mice (Figure 2D, lower panels).

To further confirm that Irs2 was deleted in the hypothalamus, especially in leptin receptor–positive areas, we performed in situ hybridization on brain sections that included the hypothalamus. We found that Irs2 expression was markedly reduced throughout the leptin receptor–positive areas in the arcuate nucleus of the hypothalamus (Figure 2E). Quantitative analyses showed Irs2 expression levels in hypothalami from βHT-IRS2 mice to be significantly decreased as compared with those in control mice (1.61 ± 0.01 kBq/g in control vs. 0.86 ± 0.05 kBq/g in βHT-IRS2, P < 0.001). To assess insulin and leptin signaling in the hypothalami of βHT-IRS2 mice, we conducted Western blot analyses. Insulin-stimulated phosphorylation of Akt in these mice was reduced to 49% of the level seen in control mice (Figure 2F, left panel). Leptin-stimulated phosphorylation of signal transducer and activator of transcription 3 (Stat3) in these mice was also reduced by 42% as compared with that in control mice (Figure 2F, right panel), suggesting that both insulin and leptin signaling were attenuated in the βHT-IRS2 hypothalamus.
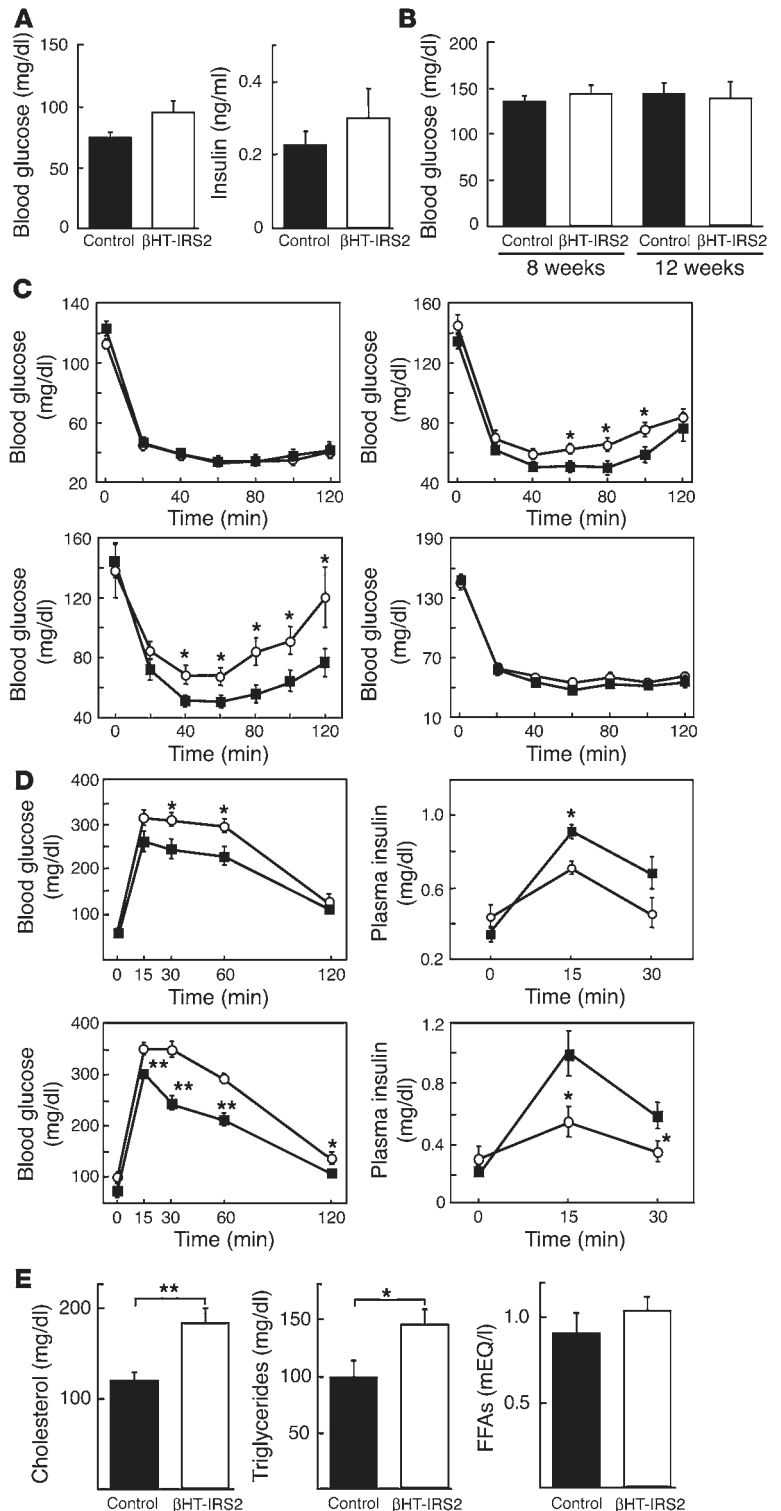
βHT-IRS2 mice show insulin resistance, glucose intolerance, and dyslipidemia. Unlike *Irs2*$^{-/-}$ mice (11, 13), the βHT-IRS2 mice did not exhibit fasting glucose and insulin elevation at 8 weeks (Figure 3A). Random blood glucose determinations yielded similar levels in βHT-IRS2 and control mice at both 8 weeks and 12 weeks (Figure 3B). Investigation of insulin sensitivity by means of insulin tolerance tests showed no significant difference between βHT-IRS2 and control mice at 4 weeks (Figure 3C, upper left panel). At 8 and 12 weeks, however, the glucose-lowering effect of insulin was significantly smaller in the βHT-IRS2 mice, suggesting that increased body weight in these mice at 8 and 12 weeks is associated with insulin resistance (Figure 3C, upper right and lower left panels). In fact, when the body weights of the βHT-IRS2 and control mice became similar during 4-week caloric restriction, the glucose-lowering effects of insulin became indistinguishable between the two groups at 8 weeks (Figure 3C, lower right panel). Next, we investigated glucose tolerance in βHT-IRS2 and control mice by means of the oral glucose tolerance tests at 8 weeks, both with caloric restriction (Figure 2D, upper panels) and without caloric restriction (Figure 2D, lower panels). After glucose loading, the blood glucose levels of both groups were significantly higher in βHT-IRS2 mice than in control mice (Figure 3D, left panels). The plasma insulin levels of both groups after the glucose load were significantly lower in βHT-IRS2 mice than in control mice (Figure 3D, right panels). These findings indicate that glucose intolerance in βHT-IRS2 mice is attributable to impaired glucose-induced insulin secretion. Assessment of lipid metabolism revealed significantly higher serum total cholesterol and triglyceride levels in βHT-IRS2 mice than in control mice (Figure 3E, left and middle panels), while their serum free fatty acid levels were similar (Figure 3E, right panel).

β Cell mass and β cell proliferation are reduced in βHT-IRS2 mice at 8 and 12 weeks. Next, we performed histological and immunohistological analyses of pancreatic islets of 8-week-old mice that had or had not been subjected to caloric restriction. We observed no insulin resistance in the former group and mild insu-

Figure 3
βHT-IRS2 mice showed insulin resistance, glucose intolerance, and dyslipidemia. (**A**) Fasting glucose (left) and insulin levels (right) of control and βHT-IRS2 mice at 8 weeks. Values are means ± SE of data obtained from the analysis of control (black bar, *n* = 12) and βHT-IRS2 mice (white bar, *n* = 13). (**B**) Random blood glucose levels of control and βHT-IRS2 mice at 8 and 12 weeks. Values are means ± SE of data obtained from the analysis of control (black bar, *n* = 12) and βHT-IRS2 mice (white bar, *n* = 13). (**C**) Insulin tolerance tests of control and βHT-IRS2 mice at 4 weeks (upper left), 8 weeks (upper right), 12 weeks (lower left), and 8 weeks with 4-week caloric restriction (lower right). Values are means ± SE of data obtained from the analysis of control (filled squares, *n* = 8–14) and βHT-IRS2 mice (open circles, *n* = 9–14). (**D**) Oral glucose tolerance tests of control and βHT-IRS2 mice at 8 weeks with caloric restriction (upper) and without caloric restriction (lower). Values are means ± SE of data obtained from the analysis of control (filled squares, *n* = 8–10) and βHT-IRS2 mice (open circles, *n* = 9–10). Blood glucose (left) and plasma insulin levels (right) were measured at the times indicated. (**E**) Serum total cholesterol (left), triglyceride (middle), and FFA (right) levels of the control and βHT-IRS2 mice at 8 weeks. Values are means ± SE of data obtained from the analysis of control (black bar, *n* = 10) and βHT-IRS2 mice (white bar, *n* = 10). *$P < 0.05$; **$P < 0.01$.
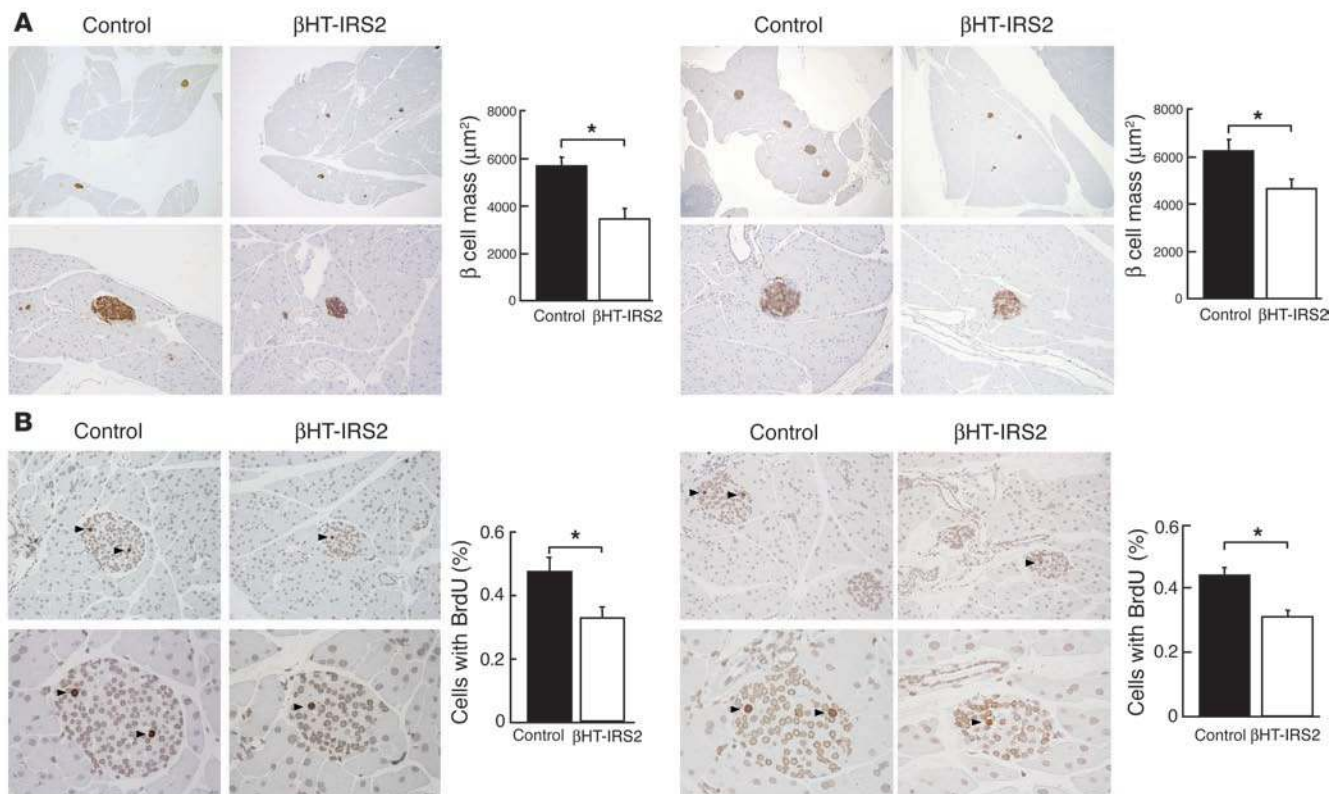
Figure 4
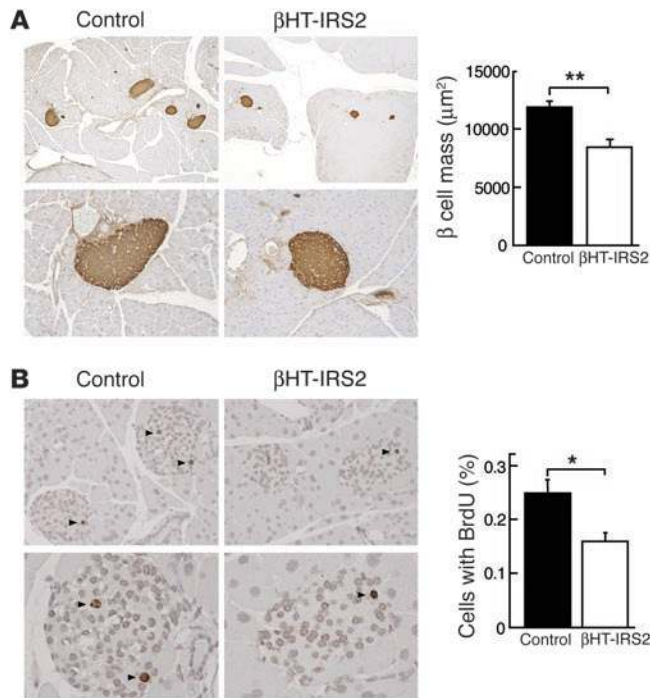β Cell mass and β cell proliferation were reduced in βHT-IRS2 mice at 8 weeks, regardless of caloric restriction. (**A**) Histological analysis of pancreatic islets (upper) and quantitation of β cell mass (lower) in control and βHT-IRS2 mice at 8 weeks with caloric restriction (left panels) and without caloric restriction (right panels). Representative islets viewed on a computer monitor are shown. Results are shown as area of β cell mass. Values are means ± SE of data obtained from the analysis of control (black bars, $n = 5$) and βHT-IRS2 mice (white bars, $n = 5$). Original magnification, ×40 (upper panels); ×100 (lower panels). (**B**) BrdU incorporation into β cell nuclei of control and βHT-IRS2 mice at 8 weeks with caloric restriction (left panels) and without caloric restriction (right panels). Results are shown as percentages of cells that incorporated BrdU. Values are means ± SE of data obtained from the analysis of control (black bars, number of islets = 192–197) and βHT-IRS2 mice (white bars, number of islets = 211–232). Original magnification, ×100 (upper panels); ×400 (lower panels). Arrowheads indicate cells that have incorporated BrdU. *$P < 0.05$.

lin resistance in the latter group (Figure 4A). The β cell mass did not differ between the groups with and without caloric restriction. Similar to the *Irs2*$^{-/-}$ mice (11, 13), however, the β cell mass of the βHT-IRS2 mice was significantly reduced as compared to that of the control mice in both groups (Figure 4A). Decreased β cell mass may be attributable to decreased proliferation and/or increased apoptosis. The percentage of cells incorporating BrdU in βHT-IRS2 mice was significantly lower than that in control mice at 8 weeks in both groups (Figure 4B), but the percentage of cells containing single-strand DNA in βHT-IRS2 mice was indistinguishable from that in control mice, both with caloric restriction (2.0% in βHT-IRS2 vs. 1.8% in control, per 100 islets) and without caloric restriction (2.1% in βHT-IRS2 vs. 2.3% in control, per 100 islets; data not shown).

We also performed histological and immunohistological analyses of pancreatic islets at 12 weeks to investigate the impact of insulin resistance. The β cell mass in βHT-IRS2 mice was significantly reduced to 72% of that in control mice (Figure 5A). Measurements of BrdU incorporation into the β cell nuclei of βHT-IRS2 and control mice (Figure 5B) indicated that a significantly lower percentage of cells in βHT-IRS2 mice incorporated BrdU, as compared to control mice (Figure 5B).

β Cell mass and β cell proliferation are not reduced in βHT-IRS2 mice at 10 days. After the decreases in β cell mass and BrdU incorporation were detected in the βHT-IRS2 mice, we performed histological and immunohistological analyses of pancreatic islets at 10 days during the breastfeeding period. The body weights of the βHT-IRS2 and control littermate mice were similar (Figure 6A). Random blood glucose determinations also yielded similar levels in the βHT-IRS2 and control littermate mice (Figure 6B). Surprisingly, the β cell masses of the βHT-IRS2 and control mice were not different (Figure 6C), and the percentages of cells incorporating BrdU did not differ significantly between the βHT-IRS2 and control mice (Figure 6D), suggesting that pancreatic β cell proliferation was not reduced in βHT-IRS2 mice at 10 days.

Normal expression of pancreas duodenum homeobox gene 1, normal insulin content, and increased insulin secretion in βHT-IRS2 mice. We next investigated the expression levels of pancreas duodenum homeobox gene 1 (Pdx1), a key transcription factor involved in pancreatic development and in the maintenance of β cell function, in the islets of βHT-IRS2 and control mice. Immunohistochemical studies revealed Pdx1 protein to be equally expressed in the nuclei of βHT-IRS2 and control mice at 8 weeks (Figure 7A, left panel) and at 12 weeks (Figure 7A, right panel). In addition, Taqman PCR

Figure 5

β Cell mass and β cell proliferation were reduced in βHT-IRS2 mice at 12 weeks. (**A**) Histological analysis of pancreatic islets (left) and quantitation of β cell mass (right) in control and βHT-IRS2 mice at 12 weeks. Representative islets viewed on a computer monitor are shown. Results are shown as area of β cell mass. Values are means ± SE of data obtained from the analysis of control (black bar, n = 5) and βHT-IRS2 mice (white bar, n = 5). Original magnification, ×40 (upper panels); ×100 (lower panels). (**B**) BrdU incorporation into β cell nuclei of control and βHT-IRS2 mice. Results are shown as percentages of cells that incorporated BrdU. Values are means ± SE of data obtained from the analysis of control (black bar, number of islets = 280) and βHT-IRS2 mice (white bar, number of islets = 284). Original magnification, ×100 (upper panels); ×400 (lower panels). Arrowheads indicate cells that have incorporated BrdU. *P < 0.05.

7D, left). However, when normalized by cell number per islet, the insulin contents of the 2 genotypes were equivalent (Figure 7D, right). We next investigated the effect of LY294002, an inhibitor of PI3K, on glucose-induced insulin secretion in βHT-IRS2 and control mice at 8 weeks. Both groups of mice exhibited similar insulin secretion with and without LY294002 at 2.8 mM glucose. At 11.1 mM glucose, insulin secretion with LY294002 in control mice was significantly higher than that without LY294002. Interestingly, insulin secretion in βHT-IRS2 mice with LY294002 was significantly higher than that without LY294002 (Figure 7E).

*βHT-IRS2 mice on a high-fat diet.* Glucose homeostasis of *Irs2^{−/−}* mice is reportedly affected by genetic background and environmental factors such as a high-fat diet (15). Therefore, we carried out a high-fat diet study in βHT-IRS2 mice. Mice were fed regular chow until

revealed the expression levels of Pdx1, hepatocyte nuclear factor 1α (Hnf1α), Hnf4α, and forkhead transcription factor 1 (Foxo1) mRNA in βHT-IRS2 and control mice to be indistinguishable at 8 weeks (Figure 7B, left panel) and at 12 weeks (Figure 7B, right panel). We then measured glucose-induced insulin secretion in βHT-IRS2 mice at 8 weeks by static incubation of the same numbers of islets for 1 hour. Whereas insulin secretions into the medium by islets from βHT-IRS2 and control mice were similar at 2.8 mM glucose, at 11.1 mM glucose, insulin secretion by islets from the βHT-IRS2 mice was significantly greater than that from control islets (Figure 7C). This remained true when we normalized the measure of glucose-induced insulin secretion by cell number (Figure 7C). There was a significant reduction in insulin content per islet in βHT-IRS2 mice as compared to that in control mice (Figure

Figure 6

β Cell mass and β cell proliferation were not reduced in βHT-IRS2 mice at 10 days. (**A**) Body weights of control and βHT-IRS2 mice. Values are means ± SE of data obtained from the analysis of control (black bar, n = 4) and βHT-IRS2 mice (white bar, n = 4). (**B**) Random blood glucose levels of control and βHT-IRS2 mice. Values are means ± SE of data obtained from the analysis of control (black bar, n = 4) and βHT-IRS2 mice (white bar, n = 4). (**C**) Histological analysis of pancreatic islets (left) and quantitation of β cell mass (right) in control and βHT-IRS2 mice at 10 days. Representative islets viewed on a computer monitor are shown. Results are shown as area of β cell mass. Values are means ± SE of data obtained from the analysis of control (black bar, n = 4) and βHT-IRS2 mice (white bar, n = 4). Original magnification, ×200. (**D**) BrdU incorporation into β cell nuclei of control and βHT-IRS2 mice. Results are shown as the percentage of cells that had incorporated BrdU. Values are means ± SE of data obtained from the analysis of control (black bar, number of islets = 67) and βHT-IRS2 mice (white bar, number of islets = 58). Original magnification, ×400 (upper panels); ×600 (lower panels). Arrowheads indicate cells that have incorporated BrdU.
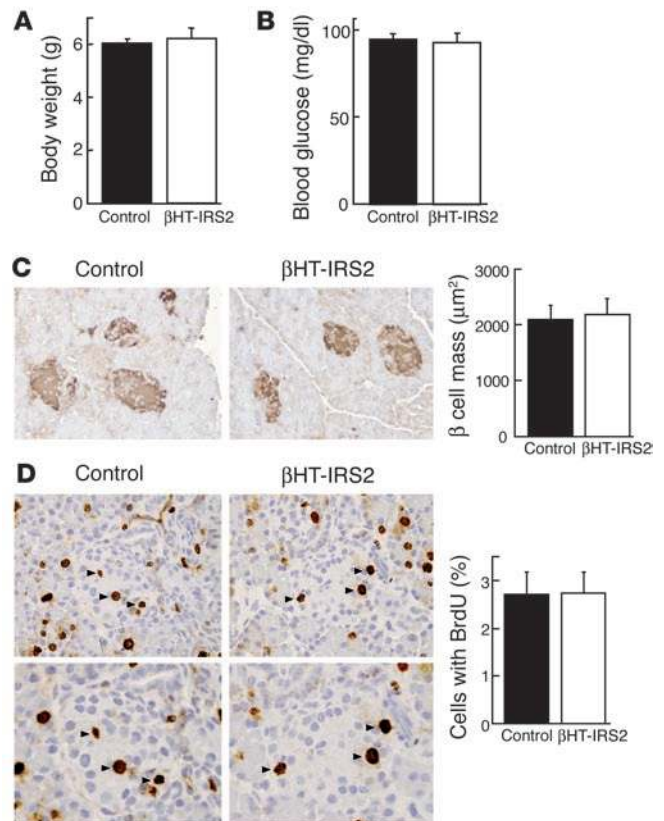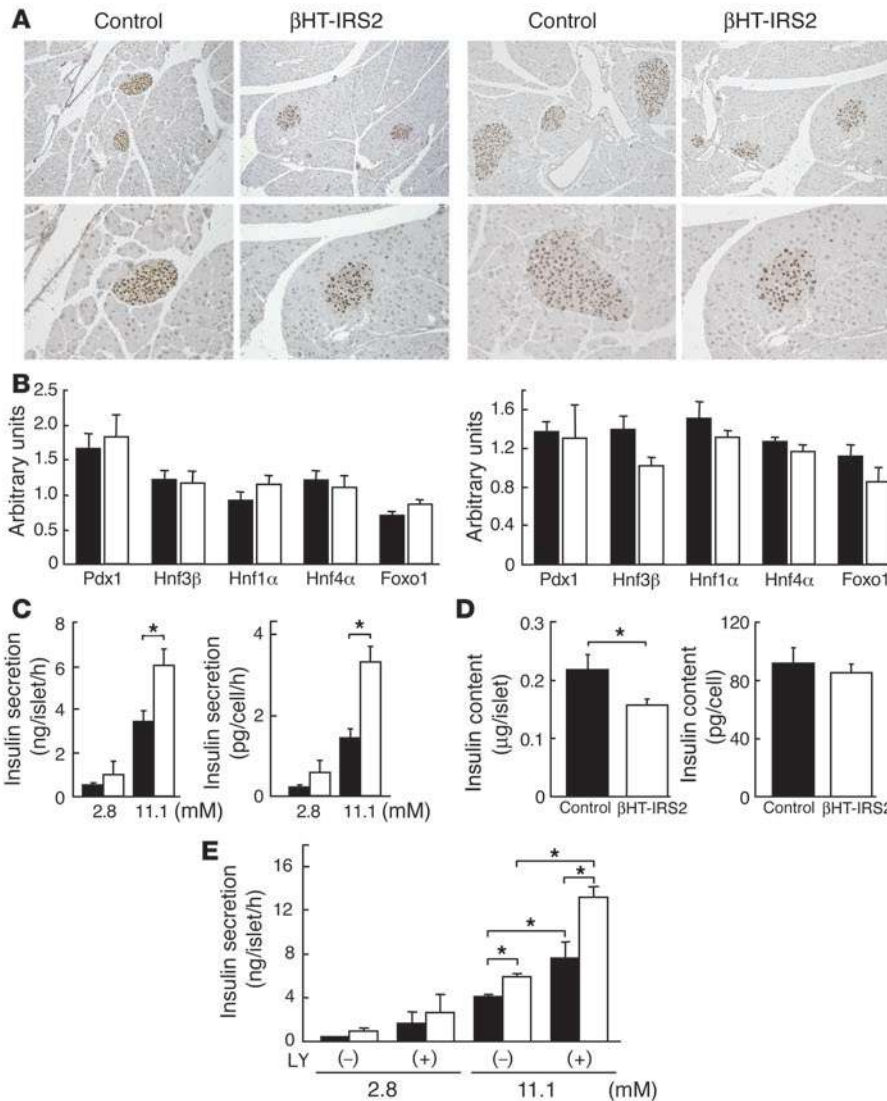
Figure 7
Normal expression of Pdx1, normal insulin contents and increased insulin secretion in βHT-IRS2 mice. (**A**) Immunohistochemical study of Pdx1 in control and βHT-IRS2 mice at 8 weeks (left panels) and at 12 weeks (right panels). Representative islets viewed on a computer monitor are shown. Original magnification ×100 (upper panels); ×200 (lower panels). (**B**) Taqman PCR analysis of Pdx1, Hnf1α, Hnf4α, and Foxo1 mRNA levels, normalized to β-actin mRNA levels in control (black bars) and βHT-IRS2 mice (white bars) at 8 weeks (left) and at 12 weeks (right). (**C**) Insulin secretion per islet (left) and insulin secretion normalized by cell number per islet (right) during static incubation of islets from control and βHT-IRS2 mice for 1 hour at the glucose levels indicated. Values are expressed as means ± SE ($n = 5$). Data were obtained in 3 independent experiments. (**D**) Insulin content per islet (left) and insulin content normalized by cell number per islet (right) in control and βHT-IRS2 mice. Values are expressed as means ± SE ($n = 5$). Data were obtained in 3 independent experiments. (**E**) Insulin secretion per islet during static incubation of islets from control and βHT-IRS2 mice for 1 hour at the glucose levels indicated with and without LY294002 (LY). Data were obtained in 3 independent experiments. *$P < 0.05$.

4 weeks of age, and then they were fed a high-fat diet for 4 weeks. The body weight and WAT mass of the epididymal fat pads of βHT-IRS2 mice were significantly higher than those of the control mice (Figure 8A). βHT-IRS2 mice developed type 2 diabetes, as fasting glucose levels were slightly but significantly higher than those of control mice (Figure 8B). In insulin tolerance tests, the glucose lowering effect of insulin was significantly lower in βHT-IRS2 mice than in control mice (Figure 8C). We performed histological and immunohistological analyses of pancreatic islets. The β cell mass of βHT-IRS2 mice was significantly reduced as compared with that of control mice (Figure 8D). We next investigated Pdx1 expression levels. Immunohistochemical studies revealed Pdx1 protein to be equally expressed in the nuclei of βHT-IRS2 mice and control mice (Figure 8E), despite the development of type 2 diabetes in the mutant mice. Taqman PCR revealed that the expression levels of Pdx1 mRNA in the βHT-IRS2 mice were slightly, but not significantly, lower than those in control mice (Figure 8F).

Discussion
We and others have demonstrated that *Irs2*^−/− mice develop type 2 diabetes as a result of an insulin signaling defect in the liver and inadequate β cell hyperplasia (11, 13), and *Irs2*^−/− mice exhibit obesity, probably due to a leptin signaling defect in the hypothalamus (12, 14). To dissect the complex and interacting pathways leading to the development of diabetes, we attempted to disrupt the *Irs2* gene in a tissue-specific fashion by using Cre-lox technology. To elucidate the role of Irs2 in β cells and the hypothalamus, we herein crossed *Irs2*^lox/lox^ mice with RIP-Cre mice (16, 17). Expression of Irs2 mRNA was markedly reduced in both islets and the arcuate nucleus of the hypothalamus, but expressions were comparable in hepatic, muscle, and adipose tissues of βHT-IRS2 and control mice. Conventional *Irs2*^−/− mice exhibited obesity associated with leptin resistance (12, 14), resulting from the attenuation of leptin signaling, which occurs with the absence of Irs2 in the hypothalamic area (18).

The striking feature of the βHT-IRS2 mice is that they exhibited a metabolic syndrome consisting of obesity, leptin resistance, insulin resistance, glucose intolerance, and dyslipidemia. Irs2 expression in βHT-IRS2 mice was markedly reduced in the arcuate nucleus area, where in situ hybridization showed leptin receptors to be densely expressed (Figure 2E), suggesting that lack of Irs2 in leptin-responsive neurons in the arcuate nucleus is the primary

cause of leptin resistance and obesity in βHT-IRS2 mice. Based on these findings, together with a recent report that Stat3 floxed mice exhibit obesity and leptin resistance (19), it seems that Stat3 and the Irs2/PI3K pathway in leptin-sensitive neurons in the arcuate nucleus are both necessary for the maintenance of normal body weight. However, the insulin receptor is known to be expressed in the arcuate nucleus area. Furthermore, insulin signaling and leptin signaling both regulate food intake and energy homeostasis (20). Since not only leptin signaling but also insulin signaling was attenuated in hypothalami from βHT-IRS2 mice (Figure 2F), we cannot rule out the possibility that a lack of Irs2 in the arcuate nucleus could lead to obesity via insulin signaling rather than leptin signaling.

βHT-IRS2 mice have a decreased β cell mass due to blunted cell growth, as manifested by decreased BrdU incorporation into DNA in β cells (Figure 4). However, at 10 days of age, both β cell mass and BrdU incorporation into DNA in the βHT-IRS2 mice and control mice were comparable (Figure 6). Irs2 may be required for some growth stimulatory signal after weaning, when the primary source of energy changes from lipids to glucose.

It has previously been demonstrated that the 129/Sv background affects diabetic phenotype, β cell morphology, and Pdx1 expression in *Irs2*−/− mice (15, 21, 22). Why did type 2 diabetes not develop in βHT-IRS2 mice despite their 129/Sv background? One possible explanation is that, unlike *Irs2*−/− mice, βHT-IRS2 mice maintained Irs2 expression in tissues other than β cells and the hypothalamus. Why were Pdx1 expression levels unaltered in βHT-IRS2 mice despite their 129/Sv background? Since *Irs2*−/− mice with the 129/Sv background showed reduced Pdx1 expression in the context of marked hyperglycemia (22), we hypothesized that reduced Pdx1 expression can be caused by a combination of 129/Sv background and hyperglycemia. Thus, we conducted a high-fat diet experiment. Although βHT-IRS2 mice developed type 2 diabetes after 4 weeks on a high-fat diet, diabetic severity was much less than that of *Irs2*−/− mice with the 129/Sv background (22). However, the expression levels of Pdx1 mRNA in the βHT-IRS2 were not significantly lower than those of control mice. Whether or not βHT-IRS2 mice show significantly decreased Pdx1 expres-

sion levels when they develop a more severe degree of hyperglycemia requires further investigation.

It is noteworthy that glucose-stimulated insulin secretion by islets was greater in βHT-IRS2 mice than it was in control mice. We initially hypothesized that the increased glucose-stimulated insulin secretion in conventional *Irs2*−/− mice was caused by insulin resistance, but the results of this study indicate that signals other than insulin resistance may be responsible for this increase. In contrast to conventional *Irs2*−/− and βHT-IRS2 mice, *Irs1*−/− mice
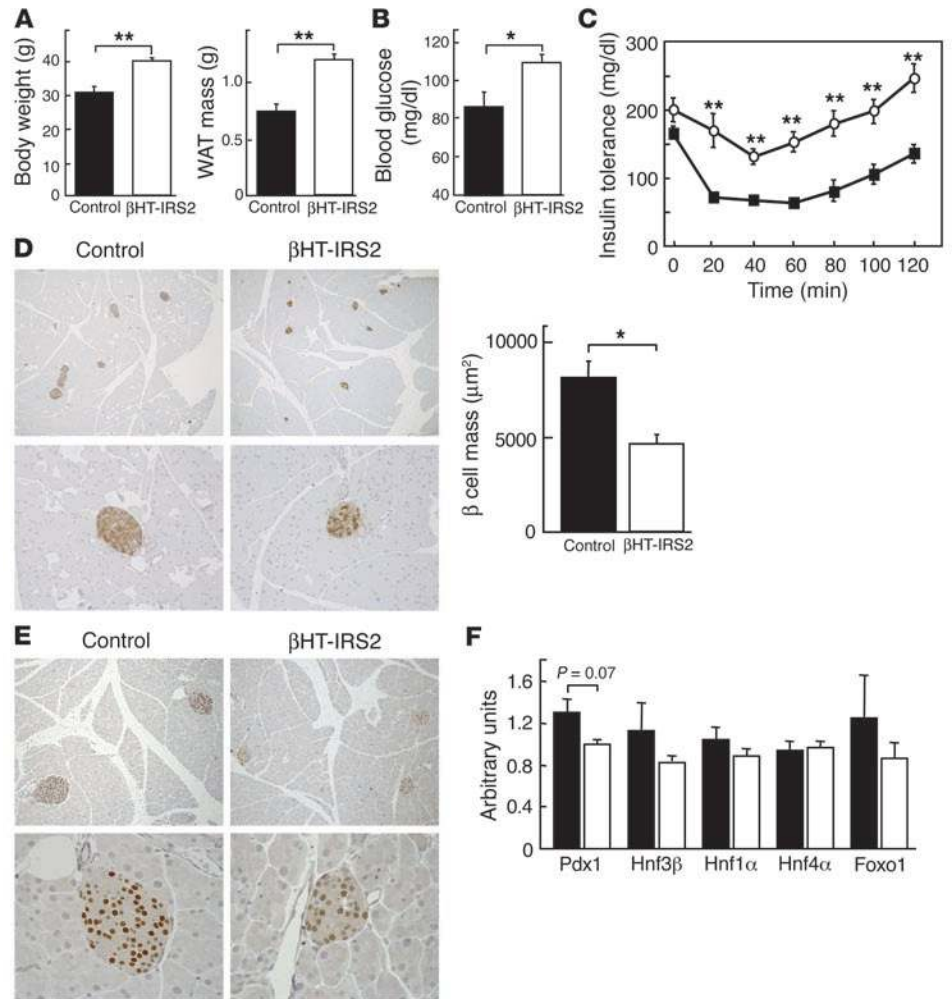
Figure 8
βHT-IRS2 mice on a high-fat diet for 4 weeks, starting from 4 weeks of age. (**A**) Body weights (left) and WAT mass of epididymal fat pads (right) of control and βHT-IRS2 mice. Values are means ± SE of data obtained from the analysis of control (black bars, *n* = 7) and βHT-IRS2 mice (white bars, *n* = 7). (**B**) Fasting blood glucose levels of control and βHT-IRS2 mice. Values are means ± SE of data obtained from the analysis of control (black bars, *n* = 7) and βHT-IRS2 mice (white bars, *n* = 7). (**C**) Insulin tolerance tests of control and βHT-IRS2 mice. Values are means ± SE of data obtained from the analysis of control (filled squares, *n* = 7) and βHT-IRS2 mice (open circles, *n* = 7). (**D**) Histological analysis of pancreatic islets (left) and quantitation of β cell mass (right) in control and βHT-IRS2 mice. Representative islets viewed on a computer monitor are shown. Results are shown as area of β cell mass. Values are means ± SE of data obtained from the analysis of control (black bar, *n* = 5) and βHT-IRS2 mice (white bar, *n* = 5). Original magnification, ×40 (upper panels); ×100 (lower panels). (**E**) Immunohistochemical study of Pdx1 in control and βHT-IRS2 mice. Representative islets viewed on a computer monitor are shown. Original magnification, ×100 (upper panels); ×200 (lower panels). (**F**) Taqman PCR analysis of Pdx1, Hnf1α, Hnf4α, and Foxo1 mRNA levels, normalized to β-actin mRNA levels in control (black bars) and βHT-IRS2 mice (white bars). *$P < 0.05$; **$P < 0.01$.

develop β cell hyperplasia but exhibit impaired glucose-stimulated insulin secretion by individual islets and β cells (7, 13, 23–25). Mutations in Irs1 in humans also lead to impaired insulin secretion (26). Moreover, β cell–specific insulin receptor KO mice show a defect in glucose-induced insulin secretion (16). β Cells from mice deficient in the PI3K p85 regulatory subunit and β cells treated with PI3K inhibitor exhibit a marked increase in the insulin secretory response to glucose (27). These findings suggest that insulin receptors acting through Irs1 stimulate insulin secretion, whereas the Irs2/PI3K pathway suppresses it. However, since insulin secretion was increased by LY294002, an inhibitor of PI3K, in βHT-IRS2 mice as well as in control mice, as we previously reported (27), the suppressive effect of Irs2 on insulin secretion is apparently not exerted through PI3K. Conventional *Irs2*−/− and βHT-IRS2 mice exhibited leptin resistance. Leptin has been reported to decrease insulin secretion (28). Thus, we cannot rule out the possibility that decreased leptin activity led to the increased insulin secretion in conventional *Irs2*−/− and βHT-IRS2 mice. In a future investigation, we plan to generate and analyze mice that are specifically deficient in Irs2 in β cells but not in the hypothalamus.

Unlike *Irs2*−/− mice, which develop diabetes at 10 weeks of age, βHT-IRS2 mice do not become diabetic. This indicates that β cell dysfunction and obesity due to hypothalamic dysfunction are insufficient for the development of diabetes. In fact, it was previously demonstrated that hepatic Irs2 restoration in *Irs2*−/− mice, using an adenoviral vector, prevented the development of diabetes (18). This observation indicates that absence of Irs2 in the hypothalamus and β cells is insufficient for the development of diabetes.

Methods

Construction of targeting vector, ES cell culture, and generation of mutant mice. To construct the targeting vectors for the *Irs2* gene, a 129/Sv mouse genomic DNA library packaged in Lambda DASH II (BD Biosciences — Clontech) was screened with 5′-side and 3′-side mouse genomic DNA as probes (probes C and B, respectively, in Figure 1A). Probe C isolated 3 clones containing *Irs2*, and probe B was used to isolate 4 clones containing this gene. We constructed 2 targeting vectors (tv's): tv-1 was the floxed neomycin-resistance gene introduced into the 3′ side of the *Irs2* gene, and tv-2 was introduced into the 5′ side (Figure 1A). First, we transfected tv-1 into J1 embryonic stem cells (129/Sv) by electroporation and screened them for homologous recombinant clones by Southern blot analysis, as described previously (29) (Figure 1B, left panel). Next, the closed circular pCre-Pac DNA was transfected by electroporation into the homologous recombinant clone to delete the floxed *neoR* of tv-1 by a method described elsewhere with minor modifications (30), and the deletion of *neoR* was confirmed by Southern blot analysis (Figure 1B, middle panel). Finally, tv-2 was electroporated into the recombinant clone lacking *neoR*, and we screened again for homologous recombinant clones by Southern blot analysis (Figure 1B, right panel).

The cells were injected into blastocysts from C57Bl/6 mice and transferred into pseudopregnant ICR females to generate chimeric mice (29). Male chimeric mice with agouti coat color were mated with C57Bl/6 female mice to generate heterozygous (*Irs2*lox/+) mice (estimated contribution of each genetic background: 50% 129/Sv and 50% C57Bl/6) (29).

Animals and genotyping. Mice were housed on a 12-hour light-dark cycle and were given either Regular Chow CE-2 (CLEA Japan Inc.) consisting of 25.6% (wt/wt) protein, 3.8% fiber, 6.9% ash, 50.5% carbohydrates, 4% fat, and 9.2% water, or High-Fat Diet 32 (CLEA Japan Inc.), consisting of 25.5% (wt/wt) protein, 2.9% fiber, 4.0% ash, 29.4% carbohydrates, 32% fat, and 6.2% water. RIP-Cre mice (C57Bl/6) were purchased from the Jack-

son Laboratory. We bred *Irs2*lox/+ mice (50% 129/Sv, 50% C57Bl/6) with RIP-Cre mice (C57Bl/6), and then bred the *Irs2*lox/+/RIP-Cre offspring (25% 129/Sv, 75% C57Bl/6) with *Irs2*lox/+ mice (25% 129/Sv, 75% C57Bl/6) to generate *Irs2*lox/lox/RIP-Cre mice (25% 129/Sv, 75% C57Bl/6), which have the same genetic background as those we used in a previous study (22). All experiments in this study were performed using littermate male mice. Genotyping was performed by PCR amplification of tail DNA from each mouse at 3 weeks of age. The primers for Cre recombinase were 5′-ACATGTTCAGGGATCGCCAGG-3′ and 5′-TAACCAGTGAAACAGCATTGC-3′, and the primers for the Irs2 and floxed Irs2 alleles were 5′-CCAGTGGGTGGCAGTGTGGGTAGG-3′, 5′-CAGCGCATCGCCTTCTATCGCCTTC-3′, and 5′-GCCATGTCCTTACAACCATTAGCGG -3′. To detect Cre-mediated recombination at the genomic DNA levels of various tissues by PCR, we designed primers for the upstream portion of Irs2 genomic DNA (primer a), Neo DNA (primer b), and the downstream portion of Irs2 genomic DNA (primer c) (see Figure 1A). Primer a was 5′-CCAGTGGGTGGCAGTGTGGGTAAGA-3′, primer b was 5′-CAGCGCATCGCCTTCTATCGCCTT-3′, and primer c was 5′-CCCATGTCTGCTTGTATGGAGAGCC-3′. These primer pairs give rise to PCR products of 0.2 kb and 0.4 kb before and after Cre-mediated Irs2 deletion, respectively. The animal care and procedures of the experiments were approved by the Animal Care Committee of the University of Tokyo.

RNA preparation and RT-PCR. Total RNA was prepared from various tissues with ISOGEN Reagent Total RNA isolation reagent (Nippon Gene Co.) according to the manufacturer's instructions. Comparative analysis of mRNA levels in different tissues was performed by RT-PCR. Total RNA was treated with RNase-free DNase (Nippon Gene Co.), and first-strand cDNA was generated with random 9-mer primers and reverse transcriptase (Takara Shuzo Co.). The reverse-transcription mixture was amplified with specific primers. The primers for Cre recombinase were as described above. The primers for Irs2 were 5′-GGTGCTAAGGTCATCCGTGCA-3′ and 5′-TTTCACGACTGTGGCTTCCTTC-3′, and the primers for 36B4 (control) were 5′-ATGCCCAGGGAAGACAGGGCGACC-3′ and 5′-TTAGTC-GAAGAGACCGAATCCCATA-3′.

Isolation of the hypothalamus. Dissections were performed on an ice-cooled glass plate. First, the rhombencephalon was separated by transverse section from the rest of the brain. A transverse section was made at the level of the optic chiasm, which delimits the anterior part of the hypothalamus and passes through the anterior commissure. The hypothalamus was dissected by using the anterior commissure as a horizontal reference, and the line between the posterior hypothalamus and the mammillary bodies was used as the caudal limit (31).

Immunoprecipitation and Western blot analysis. Immunoprecipitation and Western blot analysis were performed as described previously with some modifications (13). To assess the expression levels of Irs2, islets and hypothalami from βHT-IRS2 and control mice were homogenized, and lysates were immunoprecipitated with anti–Irs2 antibody. Samples were then separated on polyacrylamide gels and transferred to a Hybond-P PVDF transfer membrane (Amersham Biosciences).

For detection of Akt and Stat3 phosphorylation, human regular insulin (5 units/mouse) and leptin (10 mg/kg/injection) (PeproTech EC Ltd.) were injected into the tail vein after mice were fasted for more than 16 hours. Fifteen minutes after insulin and 60 minutes after leptin injection, hypothalami were homogenized, and lysates were separated on polyacrylamide gels and transferred to a Hybond-P PVDF transfer membrane (Amersham Biosciences). The membranes were incubated with the indicated antisera and HRP-conjugated anti-IgG antibodies. Bands were detected with ECL detection reagents (Amersham Biosciences).

Leptin and lipid measurements. Mice were fasted for more than 16 hours before the measurements. Serum leptin levels were determined with a

Quantikine M kit (R & D Systems Inc.). Serum total cholesterol triglyceride and free fatty acids (Wako Pure Chemical Industries Ltd.) were assayed by enzymatic methods.

Leptin sensitivity. βHT-IRS2 and control mice were injected intraperitoneally once a day at 21:00 with control saline or leptin (10 mg/kg/injection; Pepro-Tech EC Ltd.), and their body weights and food intakes were then monitored (32). The statistical significance of differences in body weight and food intake between groups was determined by Student's *t* test (2-tailed).

Caloric restriction experiment. Four-week-old βHT-IRS2 and control mice were kept in individual cages and 3.5 grams of regular chow were provided at the end of the light cycle (21:00) every day for the first week and then 4.0 grams for the second through fourth weeks. The day before starting the experiments, the mice were given ad libitum access to chow for 12 hours of the dark cycle to avoid prolonged fasting conditions.

Generation of cRNA probes for Irs2 and leptin receptor. The PCR products were ligated to the vector with a TA cloning kit (Invitrogen Corp.). ^{35}S-labeled riboprobes were generated from the fragments of PCR products for Irs2 and the leptin receptor using a Sp6/T7 transcription kit according to the manufacturer's instructions (Boehringer Mannheim GmbH). Antisense probes for Irs2 and the leptin receptor were generated by using T7 and Sp6 polymerases, respectively, and sense probes for Irs2 and the leptin receptor were generated by using Sp6/T7 polymerase (33).

In situ hybridization and histochemistry. Frozen 12-μm-thick sections from mouse brain that included the hypothalamus were cut in a cryostat at –20°C, and after thaw mounting onto gelatin-chrome alum-coated slides, these sections were stored at –80°C. Frozen tissue sections were allowed to dry in air for 10 minutes and were then fixed in 4% formaldehyde in PBS (pH 7.5) for 5 minutes and washed twice in PBS. Fixed tissue sections were incubated for 10 minutes in 0.9% saline containing 0.1 M triethanolamine and 0.25% acetic anhydride, then dehydrated by transferring them sequentially through 70% (1 minute), 80% (1 minute), 95% (2 minutes), and 100% ethanol (1 minute); and delipidated in 100% chloroform for 5 minutes. The slides were partially dehydrated in 100% ethanol (1 minute) followed by 95% (1 minute) ethanol, and allowed to dry briefly in air. Hybridization was carried out at 50°C overnight in 46 μl buffer consisting of the following: 42 μl of 23.9 mM TrisCl, 0.63 mM EDTA, 359.7 mM NaCl, 59.4% formamide, 12% dextran sulphate (500,000 mol wt), and 2.4% Denhardt's solution; 2 μl of a solution of 2.5 mg/ml sheared salmon sperm DNA (Sigma-Aldrich) and 5 mg/ml yeast total RNA (Sigma-Aldrich); and about 2 μl of ^{35}S-labeled antisense and sense probes (1 × 10^6 cpm per slide) under Nesco-film (Bando Chemical IMD) coverslips (33, 34). The slides were rinsed in 2×SSC (1×SSC: 150 mM NaCl, 15 mM sodium citrate) and washed for 30 minutes in 2 changes of 2×SSC containing 50% formamide at 50°C before being incubated at 37°C in 2×SSC containing 20 μl/ml RNase A (Sigma-Aldrich). After a further 45 minutes wash in 3 changes of 2×SSC containing 50% formamide at 50°C, the slides were washed for 10 minutes in 2 changes of 2×SSC at room temperature, and after being briefly dipped in water and 70% ethanol, they were air dried. Slides hybridized to the riboprobes were exposed to films for 3 days. Irs2 transcript hybridized sections were exposed to autoradiography film (Hyperfilm, Amersham Biosciences). The resulting images were analyzed by computerized densitometry using a MCID imaging analyzer (Imaging Research Inc.). The mean optical density of autoradiographs was measured by comparing it with simultaneously exposed [^{14}C] micro-scale samples (Amersham Biosciences).

In vivo glucose homeostasis. Glucose and insulin tolerance tests were performed according to methods described previously (32).

Histological and immunohistochemical analysis of islets. Four male mice at 10 days and five male mice at 12 weeks were used for each genotype, and sections of the pancreas were evaluated morphometrically. For the immunohistochemical analysis, pancreatic sections were stained with anti-insulin (DakoCytomation Co.) or anti–Pdx1 antibodies (35), and the areas of the islets were traced manually and analyzed with Win ROOF software (Mitani Co.) as previously described (10). More than 50 islets were analyzed per mouse in each group.

Cell proliferation. BrdU (100 mg/kg in saline) was injected intraperitoneally, and 6 hours later, the mice were perfused with 4% paraformaldehyde and their pancreata were fixed in 4% paraformaldehyde in PBS. Immunohistochemical staining techniques were performed with a Cell Proliferation Kit (Amersham Biosciences) according to a previously described method (36). For immunohistochemistry, sections were fixed in 4% paraformaldehyde for 10 minutes at room temperature, embedded in paraffin, sectioned at 2 μm, and counterstained with hematoxylin. Labeled cells and total cells in the islets were counted in 3 sections per specimen, and labeling indices were calculated as the labeled cell to total cell ratio of islets from more than 4 specimens per group.

Single-strand DNA analysis in islets. Mice were perfused with 4% paraformaldehyde and their pancreata were fixed in 4% paraformaldehyde at 4°C overnight, embedded in paraffin, and cut into 2-μm-thick sections. The sections were blocked with 10% calf serum in PBS for 20 minutes and then incubated with polyclonal antibody against single-strand DNA for 30 minutes at room temperature. Goat serum instead of single-strand DNA antibody was used for negative controls. The streptavidin-biotin complex method with an LSAB kit (DakoCytomation Co.) was used for immunohistochemistry according to the manufacturer's instructions.

Taqman PCR. Quantitative analysis of mRNA levels in islets and the hypothalamus was performed by fluorescence-based RT-PCR. The reverse-transcription mixture was amplified with specific primers using an ABI Prism 7000 sequence detector equipped with a thermocycler. The primers used for Pdx1, Hnf3β, Hnf1α, Hnf4α, Foxo1, and β-actin were as described previously (22). Relative expression levels were compared between βHT-IRS2 and control mice after normalization to β-actin.

Islet isolation and β cell preparation. Isolation of islets from mice of each genotype was carried out as described previously with some modifications (13). After clamping the common bile duct at a point close to its opening into the duodenum, we injected collagenase (Sigma-Aldrich) into the pancreatic duct. The swollen pancreas was removed and incubated at 37°C for 3 minutes. The pancreas was dispersed by pipetting, and dispersed cells were washed twice with Krebs-Ringer bicarbonate buffer. Single cells were isolated with Trypsin-EDTA (Invitrogen Corp.), as previously described (13).

Analysis of insulin content and secretion. Insulin content and secretion were measured as described previously with slight modifications (13). Isolated islets were extracted in acid ethanol at –20°C, and after preincubation with the basal glucose concentration for 20 minutes, static incubation of 10 islets/tube was performed at 37°C for 1 hour (13). Insulin levels were determined with an insulin RIA kit (Amersham Biosciences) (32). The islet cells were counted with a hemacytometer. When LY294002 was added to incubation media, it was also included in preincubation media.

Antibodies and chemicals. Rabbit polyclonal antibodies to Irs2 were purchased from Upstate Biotechnology. Rabbit polyclonal antibodies to Akt, phospho-Akt, Stat3, and phospho-Stat3 were purchased from Cell Signaling Technology. Rabbit polyclonal antibodies against single-strand DNA was purchased from DakoCytomation. LY294002 was purchased from Sigma-Aldrich.

Statistical analysis. Values are expressed as means ± SE. The statistical significance of differences between groups was determined by Student's *t* test (2-tailed).

Acknowledgments

Address correspondence to: Takashi Kadowaki, Department of Metabolic Diseases, Graduate School of Medicine, University of Tokyo, 7-3-1 Hongo, Bunkyo-ku, Tokyo 113-8655, Japan. Phone: 81-3-3815-5411 ext. 33111; Fax: 81-3-5689-7209; E-mail: kadowaki-3im@h.u-tokyo.ac.jp.

Yasuo Terauchi and Kazuyuki Tobe contributed equally to this work.

1. Kadowaki, T. 2000. Insights into insulin resistance and type 2 diabetes from knockout mouse models. *J. Clin. Invest.* **106**:459–465.
2. White, M.F. 1998. The IRS-signalling system: a network of docking proteins that mediate insulin action. *Mol. Cell. Biochem.* **182**:3–11.
3. Virkamaki, A., Ueki, K., and Kahn, C.R. 1999. Protein–protein interaction in insulin signaling and the molecular mechanisms of insulin resistance. *J. Clin. Invest.* **103**:931–943.
4. Saltiel, A.R., and Kahn, C.R. 2001. Insulin signalling and the regulation of glucose and lipid metabolism. *Nature.* **414**:799–806.
5. Nakae, J., Kido, Y., and Accili, D. 2001. Distinct and overlapping functions of insulin and IGF-I receptors. *Endocr. Rev.* **22**:813–835.
6. Shulman, G.I. 2000. Cellular mechanisms of insulin resistance. *J. Clin. Invest.* **106**:171–176.
7. Mauvais-Jarvis, F., Kulkarni, R.N., and Kahn, C.R. 2002. Knockout models are useful tools to dissect the pathophysiology and genetics of insulin resistance. *Clin. Endocrinol. (Oxf).* **57**:1–9.
8. Tamemoto, H., et al. 1994. Insulin and growth retardation in mice lacking insulin receptor substrate-1. *Nature.* **372**:182–186
9. Araki, E., et al. 1994. Alternative pathway of insulin signalling in mice with targeted disruption of the IRS-1 gene. *Nature.* **372**:186–190.
10. Terauchi, Y., et al. 1997. Development of non-insulin-dependent diabetes mellitus in the double knockout mice with disruption of insulin receptor substrate-1 and beta cell glucokinase genes. Genetic reconstitution of diabetes as a polygenic disease. *J. Clin. Invest.* **99**:861–866.
11. Withers, D.J., et al. 1998. Disruption of IRS2 causes type 2 diabetes in mice. *Nature.* **391**:900–904.
12. Withers, D.J., et al. 1999. Irs2 coordinates Igf-1 receptor-mediated beta-cell development and peripheral insulin signalling. *Nat. Genet.* **23**:32–40.
13. Kubota, N., et al. 2000. Disruption of insulin receptor substrate 2 causes type 2 diabetes because of liver insulin resistance and lack of compensatory beta-cell hyperplasia. *Diabetes.* **49**:1880–1889.
14. Tobe, K., et al. 2001. Increased expression of the sterol regulatory element-binding protein-1 gene in insulin receptor substrate-2$^{-/-}$ mouse liver. *J. Biol. Chem.* **276**:38337–38340.
15. Terauchi, Y., et al. 2003. Impact of genetic background and ablation of insulin receptor substrate (IRS)-3 on IRS-2 knock-out mice. *J. Biol. Chem.* **278**:14284–14290.
16. Kulkarni, R.N., et al. 1999. Tissue-specific knock-out of the insulin receptor in pancreatic beta cells creates an insulin secretory defect similar to that in type 2 diabetes. *Cell.* **96**:329–339.
17. Kulkarni, R.N., et al. 2002. Beta-cell-specific deletion of the Igf1 receptor leads to hyperinsulinemia and glucose intolerance but does not alter beta-cell mass. *Nat. Genet.* **31**:111–115.
18. Suzuki, R., et al. 2004. Both insulin signaling defects in the liver and obesity contribute to insulin resistance and cause diabetes in irs2$^{-/-}$ mice. *J. Biol. Chem.* **279**:25039–25049.
19. Cui, Y., et al. 2004. Essential role of STAT3 in body weight and glucose homeostasis. *Mol. Cell. Biol.* **24**:258–269.
20. Bruning, J.C., et al. 2000. Role of brain insulin receptor in control of body weight and reproduction. *Science.* **289**:2122–2125.
21. Kushner, J.A., et al. 2002. Pdx1 restores beta cell function in Irs2 knockout mice. *J. Clin. Invest.* **109**:1193–1201. doi:10.1172/JCI200214439.
22. Suzuki, R., et al. 2003. Pdx1 expression in Irs2-deficient mouse beta-cells is regulated in a strain-dependent manner. *J. Biol. Chem.* **278**:43691–43698.
23. Aspinwall, C.A., Lakey, J.R., and Kennedy, R.T. 1999. Insulin-stimulated insulin secretion in single pancreatic β cells. *J. Biol. Chem.* **274**:6360–6365.
24. Kulkarni, R.N., et al. 1999. Altered function of insulin receptor substrate-1-deficient mouse islets and cultured beta-cell lines. *J. Clin. Invest.* **104**:R69–R75.
25. Accili, D. 2001. A kinase in the life of the β cell. *J. Clin. Invest.* **108**:1575–1576. doi:10.1172/JCI200114454.
26. Porzio, O., et al. 1999. The Gly972 → Arg amino acid polymorphism in IRS-1 impairs insulin secretion in pancreatic β-cells. *J. Clin. Invest.* **104**:357–364.
27. Eto, K., et al. 2002. Phosphatidylinositol 3-kinase suppresses glucose-stimulated insulin secretion by affecting post-cytosolic [Ca(2+)] elevation signals. *Diabetes.* **51**:87–97.
28. Kulkarni, R.N., et al. 1997. Leptin rapidly suppresses insulin release from insulinoma cells, rat and human islets and, in vivo, in mice. *J. Clin. Invest.* **100**:2729–2736.
29. Kubota, N., et al. 2002. Disruption of adiponectin causes insulin resistance and neointimal formation. *J. Biol. Chem.* **277**:25863–25866.
30. Taniguchi, M., et al. 1998. Efficient production of Cre-mediated site-directed recombinants through the utilization of the puromycin resistance gene, pac: a transient gene-integration marker for ES cells. *Nucleic Acids Res.* **26**:679–680.
31. Glowinski, J., and Iversen, L.L. 1966. Regional studies of catecholamines in the rat brain. I. The disposition of [3H]norepinephrine, [3H]dopamine and [3H]dopa in various regions of the brain. *J. Neurochem.* **13**:655–669.
32. Kubota, N., et al. 1999. PPAR gamma mediates high-fat diet-induced adipocyte hypertrophy and insulin resistance. *Mol. Cell.* **4**:597–609.
33. Ueta, Y., Levy, A., Chowdrey, H.S., and Lightman, S.L. 1995. S-100 antigen-positive folliculostellate cells are not the source of IL-6 gene expression in human pituitary adenomas. *J. Neuroendocrinol.* **7**:467–474.
34. Ueta, Y., Levy, A., Chowdrey, H.S., and Lightman, S.L. 1995. Hypothalamic nitric oxide synthase gene expression is regulated by thyroid hormones. *Endocrinology.* **136**:4182–4187.
35. Offield, M.F., et al. 1996. PDX-1 is required for pancreatic outgrowth and differentiation of the rostral duodenum. *Development.* **122**:983–995.
36. Ohtsuka, N., Urase, K., Momoi, T., and Nogawa, H. 2001. Induction of bud formation of embryonic mouse tracheal epithelium by fibroblast growth factor plus transferrin in mesenchyme-free culture. *Dev. Dyn.* **222**:263–272.